A NOVEL TRANSLATIONAL MODEL FOR FETOSCOPIC INTRATRACHEAL DELIVERY OF NANOPARTICLES IN PIGLETS

Running title: fetoscopic tracheal injection in pig

Marianne S. Carlon[1]*, Alexander C. Engels[2,3]*, Barbara Bosch[2,4], Luc Joyeux[2], Marina G.M.C. Mori da Cunha[2], Dragana Vidović[1], Zeger Debyser[1], Kris De Boeck[4], Arne Neyrinck[5], Jan A. Deprest[2,3]**

[1]Molecular Virology and Gene Therapy, Department of Pharmaceutical and Pharmacological Sciences, KU Leuven, Belgium

[2]Department of Development and Regeneration, Organ System Cluster, KU Leuven, Belgium

[3]Clinical Department of Obstetrics and Gynecology, Division Woman and Child, University Hospitals Leuven, Belgium

[4]Department of Pediatric Pulmonology, University Hospitals Leuven, Belgium

[5]Laboratory of Anesthesiology and Algology, Department of Cardiovascular Sciences, KU Leuven, Belgium

*These authors contributed equally.

**Correspondence:

Jan Deprest, MD, PhD, FRCOG

Department of Obstetrics and Gynecology

University Hospital Gasthuisberg

Herestraat 49, B-3000 Leuven, Belgium

Tel: +32 16 34 42 15

Fax: + 32 16 34 42 05

E-mail: jan.deprest@uzleuven.be

Keywords: pig, fetal animal model, airway disease, cystic fibrosis, fetoscopy, micro computed tomography

Manuscript word count: 4156; 2 **tables**; 4 **figures**

What is known about this topic?

- Congenital diseases (e.g. cystic fibrosis) with high mortality or morbidity would benefit from an early intervention in the neonatal or fetal period.
- Pig lungs share many anatomical, biochemical and physiological features with human lungs.

What does this study add?

- Minimally invasive fetoscopic tracheal delivery procedures have been developed for some large animal models, but not yet for pigs.
- The model described allows therapeutics to be delivered in a translational animal species to treat diseases requiring early intervention.

Abstract

Objectives: The aim of this study was to assess the feasibility of fetal tracheal injection in the late-gestational pig to target the airways.

Methods: Following laparotomy and hysterotomy, fetoscopy was performed in pregnant sows to access the fetal trachea. Two volumes of fluospheres were injected (1 and 3 mL). Fluospheres distribution to the different lung lobes was investigated by microscopy. Possible fetal airway injury, caused by the surgical procedure or intratracheal injection, was investigated. Lung morphology and fetal lung volumes were calculated by micro computed tomography (µCT).

Results: Intratracheal administration was successfully performed in 20/21 fetuses. Analysis by confocal microscopy demonstrated that 3 mL, and not 1 mL, most efficiently targeted all lung lobes. On high-resolution µCT, total airway volume was estimated at 2.9 mL, strengthening that 3 mL is appropriate to target all lung lobes. No procedural damage was evidenced in the lungs or trachea.

Conclusions: Intratracheal injection of nanoparticles is feasible in the pregnant pig and does not cause procedural lung damage. Using an injection volume of 3 mL, all lung lobes were efficiently targeted. This nanoparticle delivery model to fetal airways opens perspectives for therapeutic interventions.

Introduction

Advances in next-generation sequencing, non-invasive procedures to isolate fetal DNA from the maternal circulation as well as high resolution ultrasound have improved first trimester diagnosis of congenital conditions [1-3]. Fetal intervention can be used to treat congenital or perinatal diseases with high mortality or morbidity if left untreated.

Cystic Fibrosis (CF) is the most common life-threatening, monogenic disease in the Caucasian population, caused by mutations in *CFTR*, coding for the Cystic Fibrosis Transmembrane Conductance Regulator protein (CFTR), a chloride/bicarbonate channel regulating fluid transport across epithelia. Although much attention goes to personalized therapy by development of mutation-specific drugs [4], gene therapy remains an attractive option since it is applicable to all patients irrespective their specific mutation [5, 6].

Patients with CF could benefit from an early intervention, starting in the neonatal or even fetal period as pathology in several organs is already apparent at birth [7]. CF animal models have been generated in different species, i.e. mouse, rat, ferret and pig [8-12]. Pig lungs share many anatomical, histological, biochemical and physiological features with human lungs [9]. While CF pigs lack lung inflammation at birth, they show impaired mucociliary clearance which leads to a failure to eradicate bacteria [13]. This leads to lung disease within the first few months of life. The relatively fast maturation rate and large number of offspring in a single sow allows fast progress in characterization of disease pathogenesis and treatment development in contrast to non-human primates, also used as a translational model for human diseases. The long life-span of pigs (10-15 years) offers advantages for evaluating long-term therapeutic efficacy of small molecules, gene therapy or engineered stem cells, and possible adverse effects that might only become apparent over time.

Before the generation of the different large animal models for CF such as pig, wild-type (WT) sheep were regularly used for translational CF gene therapy studies [14, 15]. Sheep have a similar lung size as humans, which allows the use of the same injection volume and application device for aerosol delivery to the lungs. Toxicity studies of non-viral vectors delivering hCFTR to sheep airways have demonstrated tolerability to the gene transfer agent as well as the presence of *hCFTR* mRNA in epithelial brushings or lung biopsies. The new large animal models for CF will in future allow not only the safety profile of the gene transfer agent to be evaluated, but additionally provide read-outs on the major hallmarks of CF airway disease.

Previously, we demonstrated that direct intratracheal delivery of fluospheres and viral vectors to the lungs of fetal mice resulted in more efficient targeting of lung parenchyma compared to intra-amniotic delivery [16, 17]. An efficient delivery route becomes even more important when upscaling to a large animal model, e.g. pig. Minimally invasive fetoscopic endoluminal tracheal delivery procedures

have been developed by our group for several large animal models such as sheep [18-20] and non-human primates [21].

In this study, our aim was to establish a pig model for minimally invasive fetoscopic endoluminal tracheal injection of nanoparticles, including viral vectors, stem cells or small molecules. This model would not only be applicable to study therapeutic approaches for CF, but also for other genetic disorders such as surfactant deficiency [22]. Additionally, iatrogenic conditions of the premature newborn such as bronchopulmonary dysplasia could benefit from transient overexpression of anti-oxidative proteins to reduce oxidative damage [23].

Materials and Methods

The primary goal of this study was to assess the feasibility of fetoscopic intratracheal delivery of nanoparticles in pigs. Secondary goals were the evaluation of the efficacy of intratracheal injection and the potential acute procedural-related effects on lung morphometry.

Animals Housing

Two pregnant sows (*Sus scrofa domesticus*, Belgian Landrace) were used (1-2 years, 250 kg). Animals were housed in individual stables at the Zootechnical Institute (Lovenjoel, KU Leuven, Belgium). All procedures were approved by the Animal Care and Use Committee at KU Leuven (P235-2014).

Experimental Design

Following a 2 weeks acclimation period, each sow underwent surgery at gestational age 90 (F90, 114 days for full gestation). By fetoscopic endoluminal tracheal injection, fluorescent molecules (anionic carboxylate-modified fluospheres, F8801, 100 nm, Molecular Probes, Leiden, The Netherlands) were delivered in two volumes: 1 and 3 mL. Non-injected fetuses were taken along as age-matched littermate controls. Piglets were harvested immediately post-surgery to collect lungs for further analysis.

Preoperative and Operative Care

Detailed protocols on the induction and maintenance of anesthesia are available in the online data supplement. Briefly, anesthesia was induced by intramuscular injection (0.1 mL/kg) of a mixture of zolazepam/tiletamine (Zoletil100-5 mL; Virbac s.a., Carros, France) and xylazin (Xyl-M 2%-25 mL; V.M.D.nv/sa, Arendonck, Belgium). Anesthesia was maintained by intravenous administration of ketamin (Nimatek, 100 mg/mL, Eurovet, Bladel, The Netherlands) at a constant rate perfusion of 6-10 mL/h (50 mg/mL). Fentanyl (2 µg/kg) was administered IV at 1.5 h intervals to provide intra-operative pain relief. Operated fetuses received an additional sedation mix IM into the biceps femoris (Fentanyl, 15 µg/kg; pancuronium (Pavulon), 0.4 mg/kg; Atropin, 0.1 mg/kg) at the beginning

of the injection procedure, also clinically used [24], to facilitate intratracheal injection by temporarily inhibiting breathing and swallowing reflexes and prevent bradycardia. After completion of surgery, anesthesia was stopped and T61 (0.3 mL/kg; Marion Roussel Hoechst, Brussels, Belgium) administered IV to the sow for euthanasia.

Surgical procedure

Detailed protocols on the surgical procedure are available in the online data supplement. In short, the sow was laid on the right flank after induction and general anesthesia (**Fig. 1A**). A 30 cm ventrolateral vertical skin incision was performed between the coxal tuber and the costal arch of the last rib. The fascia, external and internal abdominal oblique muscle and the peritoneum were subsequently opened. The uterus was partially elevated from the abdominal cavity. Next, gentle external pressure was applied to bring the fetal snout to a surgically accessible area away from the placenta and locate the best place for hysterostomy. Two sutures (3-0 Prolene, Johnson & Johnson Medical N.V, Diegem Belgium) were placed to fix chorion and amnion to the uterine wall at the height of the fetal snout (**Fig. 1B**). All layers of the uterine wall were opened by monopolar coagulation to generate a 1.5 cm incision. Amnion and chorion were sutured with two sutures to the uterine muscle using single stitches (3-0 Prolene). The fetal snout was held in place in front of the opening by the assisting surgeon while making sure that the mouth was submerged in amniotic fluid. Next, the fetoscopic instruments were inserted into the fetal mouth (**Fig. 1C,D**), i.e. a slightly bent 10-Fr sheath (11540 KE Karl Storz, Tutlingen, Germany) with a connection for amnio-infusion and a 1.3 mm fetoscope (11540 AA, Karl Storz). The fetoscope was connected to the light source and video recorder (20045001-DE, Tele Pack X, Karl Storz). Under constant amnio-infusion with pre-warmed (37 °C) Hartmann solution (B. Braun Melsungen AG, Melsungen, Germany), the endoscope was introduced into the fetal mouth and directed over the tongue along the midline by visualizing the raphe of the palate (**Fig. 2A**), to the pharynx, then to the larynx with the epiglottis as a landmark (**Fig. 2B**), and finally through the arytenoid cartilage and vocal cords (**Fig. 2C,D**) to the trachea (**Fig. 2E**). The landmarks appeared different than in humans [24], e.g. a separate pouch was identified dorsal of the arytenoid cartilage being the pharyngeal diverticulum (**Fig. 2C, *arrow***) and the tracheal bronchus was observed branching off the trachea (**Fig. 2E, *arrow***). The amnio-infusion was stopped after reaching the fetal trachea. Through an additional port of the fetoscopic sheath we first aspirated approximately 1.5 mL of tracheal fluid before injecting fluospheres (1 or 3 mL) into the lungs while keeping the fetoscope in place cranial to the tracheal bronchus (**Figs. 1E, 2E,F**). After injection, the fetoscope was withdrawn under visual control. The fetus was thereafter delivered through hysterotomy and a lethal dose of T61 (0.3 mL/kg) was immediately injected into the umbilical vein to prevent breathing movements while its mouth was submerged in amniotic fluid.

Macroscopic evaluation

Fetal parameters were determined at F90 (**Table 1**) on euthanized fetuses as a reference for future comparison with diseased age-matched piglets (e.g. CF piglets). Detailed procedures can be found in the online data supplement.

Determination of the optimal volume for intratracheal injection

To determine the optimal volume for intratracheal injection, we randomly chose two different volumes 1 and 3 mL (n=10/volume), based on data from adult 25-30 kg Yorkshire pigs where a 10 mL volume of treated cells was intratracheally injected [25]. Immediately post-surgery and T61 injection, the thoracic cavity was opened, the trachea ligated and the lungs removed from the body. Next, the lungs were fixed in 4% paraformaldehyde overnight at 4°C. Non-injected control fetuses were processed the same way. Samples were processed for cryosectioning as described previously [17]. Each lung sample was dissected into seven segments (i.e. left cranial and caudal lobes; right cranial, middle, accessory and caudal lobes and trachea, **Fig. 3A**). Nuclei and actin filaments were stained with DAPI (1:2000, Sigma-Aldrich, Bornem, Belgium) and Alexa Fluor 488 phalloidin (1:200, Invitrogen, Merelbeke, Belgium). Confocal images were made using a LSM 510 Meta Multiphoton microscope with ZEN 2009 software (Carl Zeiss). The relative fluorescence intensity (ratio of red to blue fluorescence representing fluospheres and nuclear staining, respectively) was quantified using ImageJ.

Histological examination of the lungs

Detailed protocols on morphometry analysis of injected piglet lungs are available in the online data supplement. In short, the acute lung injury scoring system of the American Thorax Society was applied to the different lung segments (**Fig. 3A**) as described previously [26]. Alterations of the fetal trachea were evaluated using a binomial scoring system as described before [27].

Assessment of normal lung morphology and lung volumes of the fetal lung by µCT

Although histology remains the current gold standard for lung morphometry, no three-dimensional information can be gained. This limitation makes a direct analysis of the complex 3D shapes of the small airways difficult. We therefore determined the morphological correlate of the hypothesized optimal volume for fetal intratracheal injection in the canalicular phase (F90) of lung development via µCT, a technique successfully used to study the small airways [28]. As the fetal porcine lung has not been studied by µCT before, we additionally wanted to characterize normal morphology of a wild-type pig fetus to allow future comparison with diseased fetal lungs, e.g. CF pigs. Technical details on µCT acquisition and analysis are given in the online data supplement.

Statistics

SPSS (version 21, IBM Corporation, Armonk, US) was used. One-way ANOVA was performed and a p-value < 0.05 considered significant. Data are presented as mean ± s.d.

Results

Feasibility of fetal intratracheal injection

Twenty-one of 32 fetal pigs underwent fetoscopy. All fetuses survived till harvesting (32/32). In the first sow we performed fetoscopy in 10 of 15 fetuses; in the second in 11 out of 17. Tracheoscopy was performed in all but one piglet in the first sow, in which iatrogenic tissue damage precluded the successful entrance of the trachea with the fetoscope. More specifically, the fetoscope was unintentionally inserted into the pharyngeal diverticulum which led to a false route. Therefore tracheoscopy was successful in 20 of 21 attempts and in total 20 of the 32 fetuses underwent tracheoscopy. The lungs of the remaining 12 fetuses were included as controls without tracheoscopy after the target number of fetuses was reached for tracheoscopy. All fetuses undergoing tracheoscopy were injected with 1 mL (10/20) or 3 mL (10/20) of fluospheres. The fetoscopy duration per fetus was 12.9 ± 0.7 min. The tracheal diameter was 3.7 ± 0.7 mm as measured after harvesting; the total body weight 582 ± 112.7 g and the wet lung weight 19.0 ± 5.5 g. The average crown-to-rump length was 23.4 ± 1.7 cm and the distance between nose and larynx 6.8 ± 0.6 cm **(Table 1**).

Determination of the optimal injection volume

The efficacy of fluospheres distribution throughout the different lung lobes after injection of 1 and 3 mL was evaluated by confocal microscopy (overview lung lobes, **Fig. 3A**). A representative image showing fluospheres delivery to the conducting airways and alveoli after 1 and 3 mL injection is depicted in **Fig. 3B-E**). Overall, the fluorescent intensity was higher for all lung lobes after injection of 3 mL compared to 1 mL, except for the right caudal and right accessory lobe, where mean fluorescent intensity was comparable for both volumes (**Fig. 3F**). After injection of the high volume, more fluospheres were present in central and peripheral regions. The fluorescent intensity was higher in central than in peripheral regions for the 3 mL group, whereas equal amounts of fluospheres were distributed to both regions in the 1 mL group (**Fig. 3G**). A large variability was noted between the different animals injected in both groups (n=5/group), as well as a variable efficiency in targeting the different lobes (**Fig. S1A,B**). Part of this variability could be ascribed to

pleural effusion in the low volume group in 2/5 animals (**Fig. S2**), corresponding with low amounts of fluospheres present in the lung parenchyma throughout the lung. In contrast, no pleural effusion was observed in the high volume group, although 1/5 animals showed only a low amount of fluospheres throughout the lung (**Fig. S1B**). In conclusion, comparison of two injection volumes to target the fetal lung revealed that 3 mL resulted in the highest level of fluospheres present in the different lobes, as well as in a higher level of fluospheres in central lung regions.

Analysis of procedure-related acute lung injury

The acute lung injury score was determined for the different lung lobes (**Supplementary table 1**). No difference was observed between the different lobes and no significant differences were obtained between the different treatment groups which reached a score of 2.8 % ± 0.4 % for the negative control group, 2.8 % ± 0.6 % for the 1 mL fluosphere group and 2.7 % ± 0.6 % for the 3 mL fluosphere group. Highest scores were obtained for all groups in caudal lung segments. The lowest score was obtained in all groups in the right middle lobe. The results between groups (i.e. negative controls, 1 and 3 mL fluospheres) were not significantly different (p=0.870). In the acute trachea injury score the highest value reached in any category was 2/5 animals (**Table 2**). In rare cases, abnormal results were found for loss of epithelial integrity, loss of ciliated cells and altered pars membranacea, but there was no difference between the groups. In conclusion, based on the scoring system for both the parenchyma and trachea, no acute lung injury could be observed due to the fetoscopic procedure or the different volumes injected.

Characterization of lung morphology and lung volumes by µCT

A schematic overview of the monopodial porcine airway tree is given (**Fig. 4A)**. The airway tiers (analogous to airway generations in a bipodal airway tree, cf. humans) are depicted. µCT allowed good visualization of the lungs up to the respiratory airways (**Fig. 4B**, **Movie S1**). On 10 µm resolution µCT, we analyzed two separate µCT samples of 1 cm in height and with a volume of 119.2 ± 2.2 mm^3 (**Fig. 4B,C)**. The analyzed tracheal segment, close to the carina, had a diameter of 3.8 ± 0.2 mm and a volume of 9.2 ± 0.5 mm^3. In lung tissue, we could identify 4 additional conducting airway tiers (trachea is annotated tier 0 [29]). These comprised an extra 1.9 ± 0.4 mm^3. The conducting part of the airways thus has a volume of 11.1 ± 0.02 mm^3. We subsequently analyzed the terminal bronchioles, as this region is thought to be important in the initial stages of lung pathology in CF patients [30] (**Fig. 4B-*i'***, **Movie S1** *arrows show where terminal bronchioles were calculated, i.e. at the transition point between conducting and respiratory airways*). The terminal bronchioles had a diameter of 84.3 ± 18.4 µm and cross-sectional area of 9604.2 ± 3090.2 $µm^2$. 0.68 ± 0.02 terminal bronchioles per µL lung tissue were present. The tissue percentage of the lung was 69.4%, so 29.9 mm^3 of lung tissue was made up of respiratory airways. The volume of the alveoli thus was 2.7 times higher than that of

the conducting airways (i.e. sum of tracheal segment and four conducting airway tiers). To estimate the total airway volume of the entire lung, the right lung was subsequently scanned at a resolution of 17.6 µm, resulting in 4.9 cm^3 total lung volume. Based on our data found at high resolution, the volume of the respiratory airways in the right lung can thus was estimated at 1.2 mL and that of the conducting airways at 0.5 mL, which together comprise an estimated right lung airway volume of 1.7 mL. As the right to left lung ratio was 1.38 ± 0.01 g (based on dry lung weights of three fetal lungs), total airway volume of both lungs could be estimated at 2.9 mL, which strengthens the observation that the highest volume of fluospheres (3 mL) resulted in widespread targeting of the different lobes (**Fig. 3**).

Discussion

In this manuscript we demonstrate that intratracheal fetoscopic application of nanoparticles in F90 fetuses at hysterotomy, validated here by fluospheres, is possible in the pig. Fluospheres distribution was successful in all but one case at the beginning of our experience where a false route was taken (20/21 injected piglets). In the others, the intervention had no measureable acute effects on the fetuses or their lungs. We could identify most efficient nanoparticle delivery in all lung lobes after 3 mL injection, however with notable variation between lung areas and in between animals. Based on high-resolution µCT, total airway volume was estimated at approximately 2.9 mL, strengthening that the 3 mL volume is appropriate to target all lung lobes.

Different animal models have been described for intra-uterine nanoparticles delivery into fetal lungs [17-21, 31, 32]. Only larger animals, such as sheep, pig and primates allow the fetoscopic route due to their comparable anatomical size as humans. Fetoscopic application has the advantage that visual control allows correct airway delivery. We demonstrated that fetal tracheoscopy in pig is feasible and that injection of different volumes does not lead to measurable acute lung injury or tracheal damage. Additionally, local administration to the airways by direct intratracheal injection allows a lower dose to be administered compared to the technically easier intra-amniotic delivery, which is especially important in large animal models requiring large volumes injected. Compared to sheep and primates, pigs have the advantage having multigestational pregnancies of 8 to 12 piglets. Therefore more fetuses per sow can be used which reduces the number of animals needed for experimentation, as well as increases the number of internal littermate controls.

We are aware of certain limitations in our study, one being the use of only two sows. However, our primary goal was to evaluate fetal tracheoscopic delivery, which we could apply in 21 fetuses. Thanks to the large litter size, we harvested another 12 controls. Another shortcoming is the short latency between operation and harvesting which was approximately 5-10 minutes. Again however,

our goal was to study the distribution of fluospheres following intratracheal delivery which inherently has to be studied as soon as possible after administration. On the other hand, studying the pharmacokinetics of the distributed nanoparticles is important as well, but this will depend strongly on the exact characteristics of the given nanoparticle. For example, viral vectors on average can enter a target cell in a short time frame (minutes-hours) [33], whereas for other nanoparticles such as stem cells it will be important that they can reside at the desired lung region for a longer time period (hours, days) [34]. A next step towards the development of a preclinical animal model that allows long-term evaluation of the administered nanoparticle will require the development of an optimal surgical procedure that allows survival of the operated sow and piglets. In contrast to the present study, long-term experiments would necessitate the closure of the hysterotomy and laparotomy, which would lead to a considerably longer duration of surgery and potentially increase the risk of unsuccessful closure or wound healing complications. In general, pregnant sows are susceptible to stress-related abortion, that will have to be taken into account when optimizing the surgical procedure combining it with an optimal anesthesia protocol and minimal surgery duration [35]. To eventually translate fetal delivery experiments in WT pigs to gene therapy studies in the CF pig, toxicity and gene expression analyses will have to be optimized, assays already operational in sheep [14, 15]. However, many CF specific read-outs have recently been developed that allow assessment of the major hallmarks of CF airway disease in large animal models, such as mucociliary clearance, airway surface liquid depth and bacterial killing [13, 36, 37]. Ultimately, combining all these read-outs will provide a complete overview of the safety and efficacy of novel therapies for CF.

Another interesting point is whether fluosphere delivery is fully representative of predicting other nanoparticles' biodistribution, as they might have different physicochemical properties. Fluosphere distribution depends on the particle size and the adhesion properties. For this study, we used 100 nm anionic carboxylate-modified fluospheres, diluted 1:2 in saline, as they are superior for applications in biological systems. As they are highly charged, this reduces their attraction to negatively charged cell surfaces. Viral vector biodistribution depends on several factors, including vector size (e.g. 20 nm for rAAV), the substance it is dissolved in, usually saline, and its tropism. In the past we have already shown that the distribution of fluospheres was very comparable to that of rAAV2/6.2 delivery and subsequent gene expression in fetal mouse airways [16, 17].

The delivery of two different fluospheres volumes (1 and 3 mL) allowed us to determine the optimal injection volume. Confocal analysis revealed that the high volume resulted in the highest level of fluospheres present in the different lung lobes. However, a large variability was noted between the different animals injected for both groups, as well as a variable efficiency in targeting the different lobes. In some of the animals with low amounts of fluospheres present in the lung parenchyma,

pleural effusion was noted. In none of the injected fetuses, spilling of fluospheres through the oropharynx was observed during administration. The 3 mL injection volume at first sight exceeds the total airway volume estimate of 2.9 mL. However, in this calculation only the distal trachea was included, whereas injection took place cranially to the tracheal bronchus. Therefore an excess of fluospheres was most likely not injected, even with the high volume. Additionally, lung fluid was aspirated prior to injection. Alternatively, leakage could have occurred due to procedural damage, i.e. placement of the fetoscope or the injected volumes. However, in the acute lung injury score no damage to trachea or parenchyma was evidenced, although small or local lesions could have been missed as the score is calculated on 5 high power fields per region per animal. We cannot exclude that leakage could have occurred while processing the whole lung into the different lung samples for microscopic analysis on frozen sections. This is something that will be taken into account in future experiments. Overall, 3 mL injection efficiently targeted the different lobes, suggesting this volume as appropriate for future administrations at this gestational age.

These findings were strengthened by µCT where the total airway volume was estimated at approximately 2.9 mL based on detailed volume calculations of the conducting and respiratory airways combined with lower resolution µCT to determine the total lung dimension. Important to point out is that, to our knowledge, this is the first time a fetal pig lung is imaged by µCT. This pioneering comes with some intrinsic uncertainties. First, we found a high tissue percentage of 69.4% compared to 30.6% air-filled space (expressed as fluid-filled space in a fetal setting). In human adult lung, the tissue percentage is approximately 20% based on µCT imaging using osmium as tissue contrast enhancement agent [38]. This might be because of incomplete removal of liquid from the fetal lung or the inherent properties of the fetal lung at this specific lung developmental stage. The percentage of fluid-filled space measured by µCT ultimately impacts the airway volume calculations and errors at this stage will influence the value for the total airway volume, here estimated at 2.9 mL. Also, there is no clear consensus on which terminology to use for labeling the different pig airways. Due to anatomical differences in branching pattern of human and pig conducting airways, i.e. a bipodal versus monopodial airway tree, the human nomenclature is not suited. In that light, Bauer and colleagues introduced a new terminology to more accurately label the porcine conducting airways [29]. As an analog to human airway generations, they propose “airway tiers” (for a schematic overview see **Fig. 4A**).

In conclusion, we demonstrated for the first time in a pregnant pig that intratracheal injection of nanoparticles is feasible via fetoscopy at hysterotomy. This delivery procedure to fetal airways opens up perspectives to further study the effect of nanoparticle delivery in a large fetal animal model.

Acknowledgments

We would like to thank Rosita Kinnart, Ivan Laermans and Stijn Massart for their help with the *in vivo* experiments and Myrthe Boijmans for illustrating the surgical procedure. We would also like to thank Liesbeth De Keersmaecker and Marjolein Ensinck for their help with processing and quantification of injected fetal pig lungs. M.S.C. is a postdoctoral fellow supported by the "Fund Alphonse and Jean Forton", King Baudouin Foundation, Belgium [3M140231]. The work was supported by an Innovative Engineering for Health award by Wellcome Trust [WT101957], the Engineering and Physical Sciences Reserach Council (EPSRC) [NS/A000027/1] as well as the Fonds Wetenschappelijk Onderzoek Vlaanderen (FWO) [18.01207] and the Erasmus + Program of the European Union (Framework agreement number 2013-0040; contract 1011990).

Disclosure conflict of interest

No conflicts of interest.

References

1. Metzker ML. Sequencing technologies - the next generation. Nat Rev Genet 2010; 11:31-46.
2. Morain S, Greene MF, Mello MM. A new era in noninvasive prenatal testing. N Engl J Med 2013; 369:499-501.
3. Katorza E, Achiron R. Early pregnancy scanning for fetal anomalies--the new standard? Clin Obstet Gynecol 2012; 55:199-216.
4. Bell SC, De Boeck K, Amaral MD. New pharmacological approaches for cystic fibrosis: promises, progress, pitfalls. Pharmacol Ther 2015; 145:19-34.
5. Vidovic D, Carlon MS, da Cunha MF*, et al.* rAAV-CFTRDeltaR Rescues the Cystic Fibrosis Phenotype in Human Intestinal Organoids and Cystic Fibrosis Mice. Am J Respir Crit Care Med 2016; 193:288-98.
6. Armstrong DK, Cunningham S, Davies JC*, et al.* Gene therapy in cystic fibrosis. Arch Dis Child 2014; 99:465-8.
7. Rowe SM, Miller S, Sorscher EJ. Cystic fibrosis. N Engl J Med 2005; 352:1992-2001.
8. Klymiuk N, Mundhenk L, Kraehe K*, et al.* Sequential targeting of CFTR by BAC vectors generates a novel pig model of cystic fibrosis. J Mol Med (Berl) 2012; 90:597-608.
9. Rogers CS, Hao Y, Rokhlina T*, et al.* Production of CFTR-null and CFTR-DeltaF508 heterozygous pigs by adeno-associated virus-mediated gene targeting and somatic cell nuclear transfer. J Clin Invest 2008; 118:1571-7.
10. Sun X, Sui H, Fisher JT*, et al.* Disease phenotype of a ferret CFTR-knockout model of cystic fibrosis. J Clin Invest 2010; 120:3149-60.
11. Tuggle KL, Birket SE, Cui X*, et al.* Characterization of defects in ion transport and tissue development in cystic fibrosis transmembrane conductance regulator (CFTR)-knockout rats. PLoS One 2014; 9:e91253.
12. Wilke M, Buijs-Offerman RM, Aarbiou J*, et al.* Mouse models of cystic fibrosis: phenotypic analysis and research applications. J Cyst Fibros 2011; 10 Suppl 2:S152-71.

13. Hoegger MJ, Fischer AJ, McMenimen JD*, et al.* Cystic fibrosis. Impaired mucus detachment disrupts mucociliary transport in a piglet model of cystic fibrosis. Science 2014; 345:818-22.
14. Alton EW, Baker A, Baker E*, et al.* The safety profile of a cationic lipid-mediated cystic fibrosis gene transfer agent following repeated monthly aerosol administration to sheep. Biomaterials 2013; 34:10267-77.
15. McLachlan G, Davidson H, Holder E*, et al.* Pre-clinical evaluation of three non-viral gene transfer agents for cystic fibrosis after aerosol delivery to the ovine lung. Gene Ther 2011; 18:996-1005.
16. Carlon M, Toelen J, Van der Perren A*, et al.* Efficient gene transfer into the mouse lung by fetal intratracheal injection of rAAV2/6.2. Mol Ther 2010; 18:2130-8.
17. Carlon MS, Toelen J, da Cunha MM*, et al.* A novel surgical approach for intratracheal administration of bioactive agents in a fetal mouse model. J Vis Exp 2012.
18. Aubry E, Fayoux P, Jani J*, et al.* Tracheal occlusion alters pulmonary circulation in the fetal lamb with normally developing lungs. J Pediatr Surg 2013; 48:481-7.
19. Deprest JA, Evrard VA, Van Ballaer PP*, et al.* Tracheoscopic endoluminal plugging using an inflatable device in the fetal lamb model. Eur J Obstet Gynecol Reprod Biol 1998; 81:165-9.
20. Luks FI, Deprest JA, Vandenberghe K*, et al.* Fetoscopy-guided fetal endoscopy in a sheep model. J Am Coll Surg 1994; 178:609-12.
21. Mari G, Deprest J, Schenone M*, et al.* A novel translational model of percutaneous fetoscopic endoluminal tracheal occlusion - baboons (Papio spp.). Fetal Diagn Ther 2014; 35:92-100.
22. Aneja MK, Rudolph C. Gene therapy of surfactant protein B deficiency. Curr Opin Mol Ther 2006; 8:432-8.
23. Richter J, Toelen J, Vanoirbeek J*, et al.* Functional assessment of hyperoxia-induced lung injury after preterm birth in the rabbit. Am J Physiol Lung Cell Mol Physiol 2014; 306:L277-83.
24. Deprest J, Gratacos E, Nicolaides KH*, et al.* Fetoscopic tracheal occlusion (FETO) for severe congenital diaphragmatic hernia: evolution of a technique and preliminary results. Ultrasound in obstetrics & gynecology : the official journal of the International Society of Ultrasound in Obstetrics and Gynecology 2004; 24:121-6.
25. Gui L, Qian H, Rocco KA*, et al.* Efficient intratracheal delivery of airway epithelial cells in mice and pigs. Am J Physiol Lung Cell Mol Physiol 2015; 308:L221-8.
26. Matute-Bello G, Downey G, Moore BB*, et al.* An official American Thoracic Society workshop report: features and measurements of experimental acute lung injury in animals. American journal of respiratory cell and molecular biology 2011; 44:725-38.
27. Deprest JA, Evrard VA, Verbeken EK*, et al.* Tracheal side effects of endoscopic balloon tracheal occlusion in the fetal lamb model. European journal of obstetrics, gynecology, and reproductive biology 2000; 92:119-26.
28. Boon M, Verleden SE, Bosch B*, et al.* Morphometric Analysis of Explant Lungs in Cystic Fibrosis. Am J Respir Crit Care Med 2015.
29. Bauer C, Adam R, Stoltz DA*, et al.* Computer-aided analysis of airway trees in micro-CT scans of ex vivo porcine lung tissue. Comput Med Imaging Graph 2012; 36:601-9.
30. Tiddens HA, Donaldson SH, Rosenfeld M*, et al.* Cystic fibrosis lung disease starts in the small airways: can we treat it more effectively? Pediatr Pulmonol 2010; 45:107-17.
31. DeKoninck P, Toelen J, Roubliova X*, et al.* The use of human amniotic fluid stem cells as an adjunct to promote pulmonary development in a rabbit model for congenital diaphragmatic hernia. Prenatal diagnosis 2015; 35:833-40.
32. Mayer S, Klaritsch P, Sbragia L*, et al.* Maternal administration of betamethasone inhibits proliferation induced by fetal tracheal occlusion in the nitrofen rat model for congenital diaphragmatic hernia: a placebo-controlled study. Pediatr Surg Int 2008; 24:1287-95.
33. Lakadamyali M, Rust MJ, Babcock HP*, et al.* Visualizing infection of individual influenza viruses. Proc Natl Acad Sci U S A 2003; 100:9280-5.

34. Mori da Cunha MGMC, Zia S, Beckmann DV*, et al.* VEGF upregulation in human amniotic fluid stem cell enhances nephroprotection after ischemia-reperfusion injury in the rat. Critical Care Medicine 2016; in press.
35. Hutchings LM. Abortion in swine. Vet Med 1946; 41:99-101.
36. Stoltz DA, Meyerholz DK, Pezzulo AA*, et al.* Cystic fibrosis pigs develop lung disease and exhibit defective bacterial eradication at birth. Sci Transl Med 2010; 2:29ra31.
37. Birket SE, Chu KK, Liu L*, et al.* A functional anatomic defect of the cystic fibrosis airway. Am J Respir Crit Care Med 2014; 190:421-32.
38. Kampschulte M, Schneider CR, Litzlbauer HD*, et al.* Quantitative 3D micro-CT imaging of human lung tissue. Rofo 2013; 185:869-76.

Tables

Table 1: Fetal macroscopic parameters

GROUP	Tracheal diameter (mm)	Total body weight (g)	Wet lung weight (g)	Crown-to-rump length (cm)	Nose-to-larynx (cm)
Control	3,7 ± 0,7	544,9 ± 120,6	15,9 ± 3,3	22,8 ± 1,6	6,5 ± 0,6
Fluospheres 1 mL	3,9 ± 0,6	605,8 ± 105,0	23,1 ± 5,9	23,7 ± 1,5	6,8 ± 0,5
Fluospheres 3 mL	3,6 ± 0,6	602,7 ± 97,5	18,6 ± 4,5	23,7 ± 1,6	6,9 ± 0,5

Fetal parameters were determined for 32 piglets (n=12 neg. controls; n=10 fluospheres 1 mL; n=10 fluospheres 3 mL) at F90 after euthanasia and removal from the uterus. Macroscopic outcomes are reported for all fetuses and the calculated means ± s.d. given.

Table 2: Acute tracheal injury score

GROUP	[a]Epithelium integrity	[b]Epithelium qualitative	[c]Epithelium folding	[d]Submucosal reaction	[e]Cartilage viability	[f]Pars membranacea
Control	1/5	2/5	0/5	0/5	0/5	1/5
Fluospheres 1 mL	1/5	1/5	0/5	0/5	0/5	1/5
Fluospheres 3 mL	1/5	1/5	0/5	0/5	0/5	1/5

The numbers shown are positive cases (n) of total cases per treatment group (5). The influence of intratracheal injection on the tracheal tissue was evaluated as in [27]. Explanation of the different outcomes: [a]Epithelium integrity: 0 = Intact, 1 = defect; [b]Epithelium qualitative: 0 = normal ciliary epithelium, 1 = Squamous metaplasia; [c]Epithelium folding : 0 = normal folding, 1 = unfolding or compression; [d]Submucosal acute inflammatory reaction: 0 = absent, 1 = infiltration of neutrophils; [e]Cartilage viability: 0 = normal, 1 = cartilage destruction or deformity; [f]Pars membranacea: 0 = normal, 1 = intramural/transmural rupture of muscle.

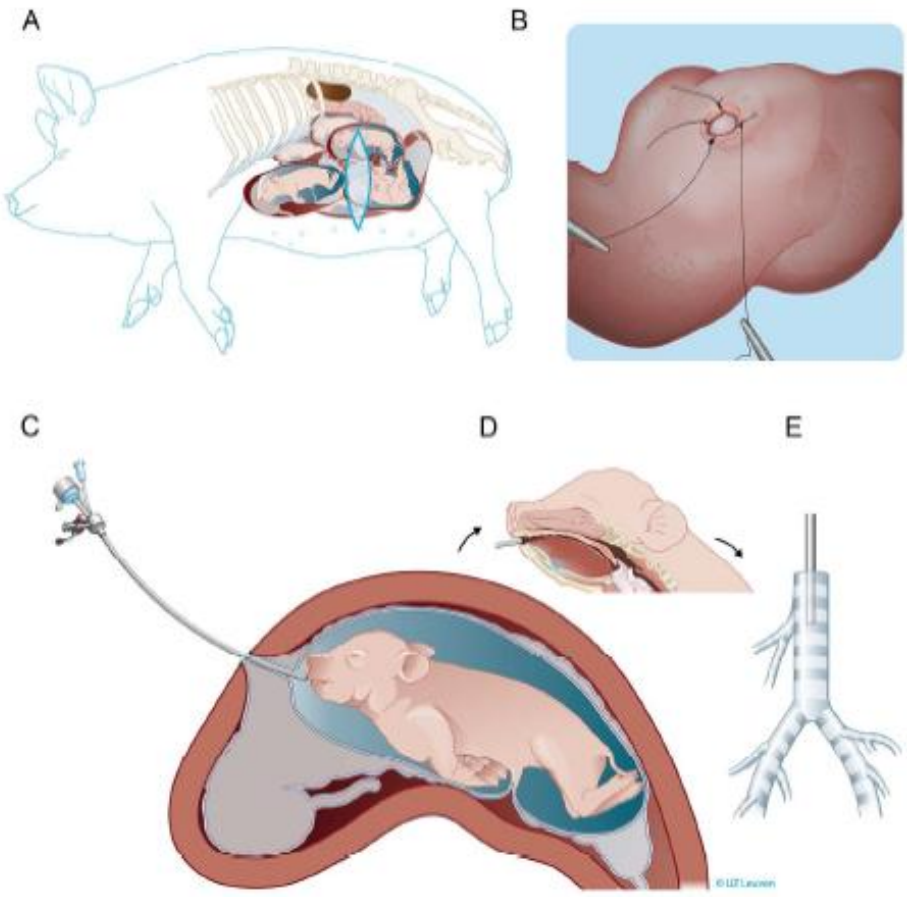

Figure 1: Schematic overview of the fetal surgical procedure. (A) The sow was anesthetized and positioned on the right flank. Afterwards a vertical flank incision was performed to expose the uterus. The fetal position was evaluated by ultrasound and two initial sutures were made above the fetal snout. (B) The uterus, including the fetal membranes, was opened and two additional stiches were placed to fix amnion and chorion to the uterus. (C) Next, the fetoscopic instruments were inserted into the fetal mouth by holding the mouth in position in front of the hysterostomy. (D) The fetoscope was directed over the tongue along the midline by visualizing the different landmarks as described in figure 2 and (E) finally positioned in the cranial part of the fetal trachea.

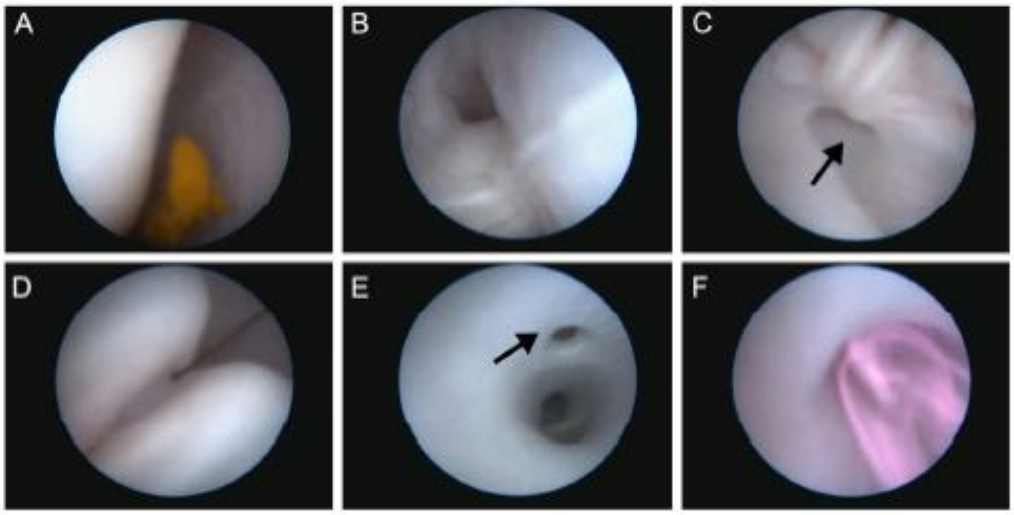

Figure 2: Fetoscopic endoluminal tracheal injection of fluospheres. (A) After entering the fetal mouth with the fetoscope, the midline and raphe of the palate can be identified. Next, the (B) epiglottis and (C) arytenoid cartilage of the larynx and subsequently (D) the vocal cords could be identified, as well as a separate pouch dorsal of the arytenoid cartilage being the pharyngeal diverticulum (C, arrow). Finally, the fetoscope was positioned in the trachea proximal of the tracheal lobe bronchus (E, arrow) where after the fluospheres were injected (F).

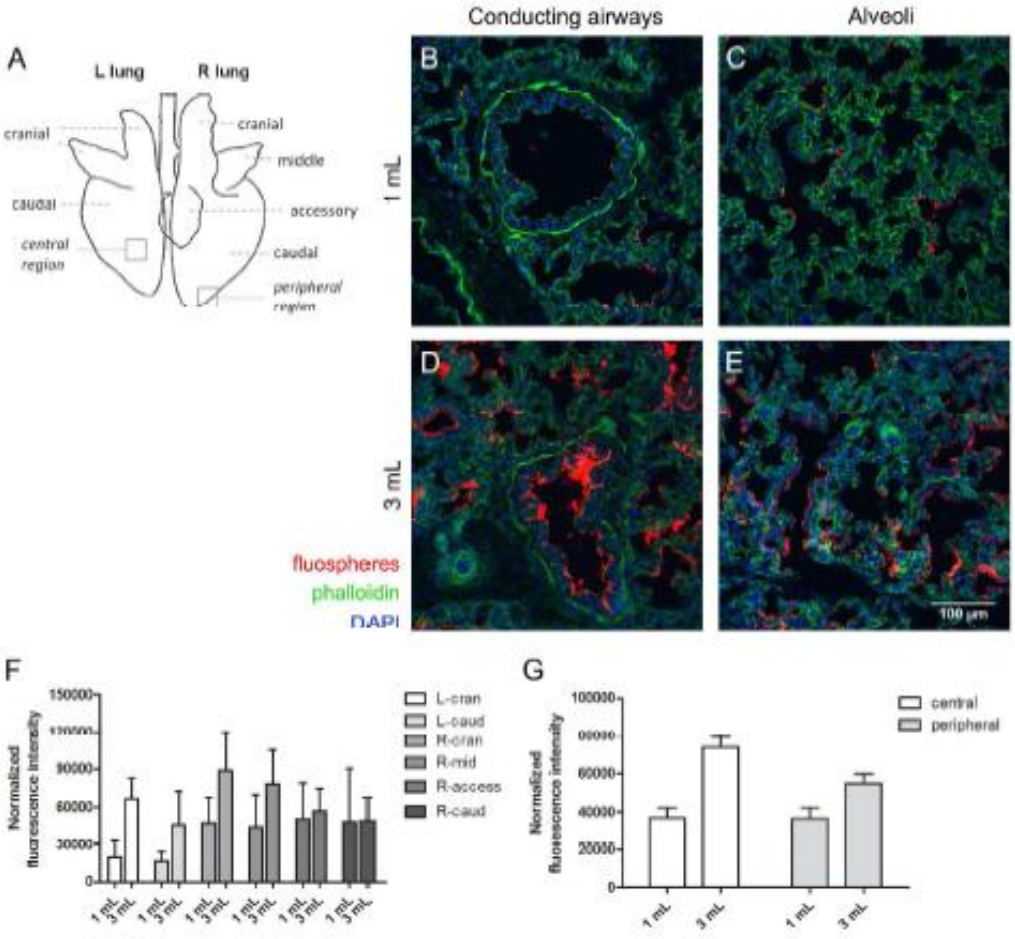

Figure 3: Quantification of fluospheres distribution in the different lung regions. (A) Schematic overview of the different lung lobes in pig. Representative images of the F90 piglet lung injected with 1 mL (B-C) and 3 mL (D-E) of fluospheres (red). F-actin was visualized using phalloidin-488 (green); nuclei were stained with DAPI (blue). (F) Quantification of the relative fluorescence intensity in the different lung regions by calculating the ratio of fluospheres to the total cell content (measured by DAPI fluorescence). (G) Quantification of the average relative fluorescence intensity in central and peripheral lung regions based on values obtained for the different lung lobes. Data are presented as mean ± s.e.m.

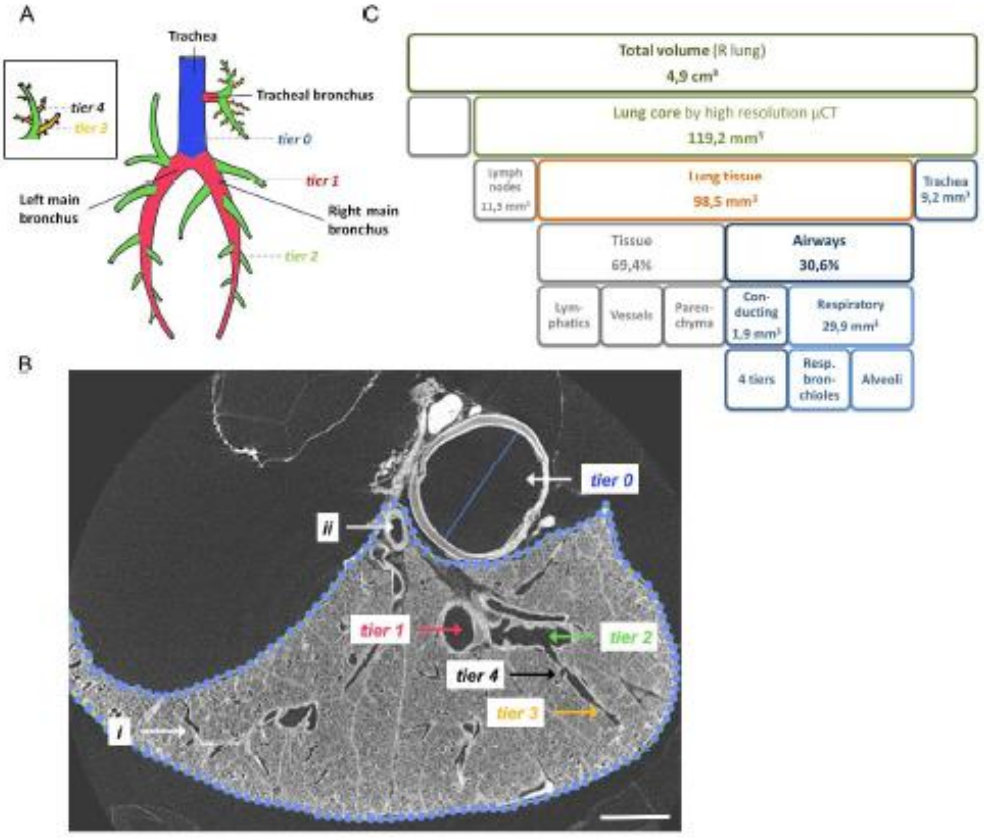

Figure 4: µCT imaging allows morphometric analysis of the F90 pig lung. (A) Schematic overview of the monopodial airway tree of the pig. The airway tiers (analogous to airway generations in a bipodal airway tree, cf. humans) are depicted. When an airway branches into two airways, the smaller airway gets the tier level of the parental branch plus one. An exception to this rule is the tracheal bronchus (tier 1), that gives rise to two tier 2 branches, a cranial and a caudal one. The trachea is annotated tier 0 (blue). All airways that branch directly of the trachea are tier level 1 (red). Tier 2 airways (green) branch directly off the tier 1 airways and tier 3 airways (orange) off the tier 2 branches. (B) Within the lung tissue (dotted line) on a cross-sectional image, we can identify 4 conducting airway tiers (tier 1-4) ending in the terminal bronchioles (i), which is the transition between conducting and respiratory airways. The volume of the large vessels within the lung can be calculated (ii) as well as the dimension of the trachea (tier 0). (C) µCT measurements with a resolution of 10 µm allowed computing of conducting and respiratory airway volumes based on two cores of 119 mm3. Subsequently, a µCT scan at 17.6 µm resolution was performed to determine the total lung dimension of the right lung. Panel A is adapted from reference 29. Scale bar in panel B is 2 mm.